# PROGRESS OF THE DIAGNOSTICS AT THE PROSCAN BEAM LINES

R. Dölling, PSI, Villigen, Switzerland

*Abstract*

Operation experience, improvements and new variants of the PROSCAN beam line diagnostics as well as an improved profile-evaluation technique are reported.

## INTRODUCTION

PROSCAN, the dedicated new medical facility at PSI using proton beams for the treatment of deep seated tumours and eye melanoma, has restarted routine operation with Gantry 1. Further beam lines will be commissioned in this year. Air and $N_2$ filled ionisation chambers (IC) and secondary emission monitors (SEM) in several configurations are used as current, profile, halo, position and loss monitors (Fig. 1, [1, 2]). New variants of a multi-leaf Faraday cup (MLFC) and an IC position monitor will be used at the beam line to OPTIS 2.

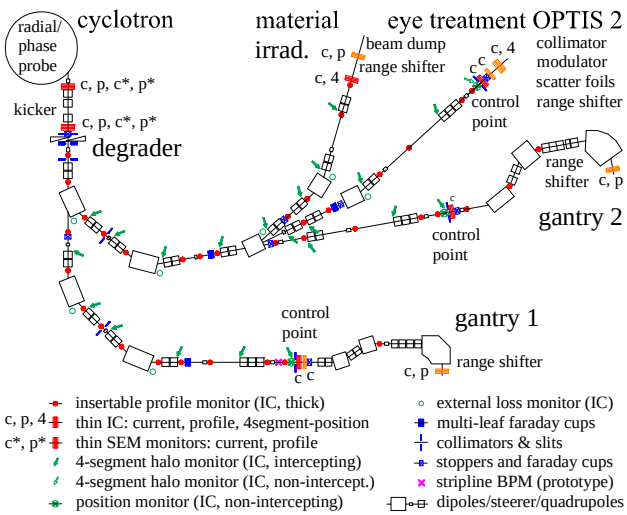


Figure 1: Overview of beam lines and diagnostics.

## STATUS AND OPERATION EXPERIENCE

During commissioning and operation, the diagnostics performed as intended. It contributed only negligibly to the unscheduled down time of the facility. The sensitivity, accuracy and speed of the various IC monitors fully suit the requirements. Comprehensive online beam information as well as fast surveillance options are already available, but are not fully used in the present stadium of the project. The self-tests of the diagnostics are still unavailable, awaiting changes in the logarithmic amplifier modules and support by the control system.

The thin IC current and profile monitors in front of the degrader are, together with the thin current monitors at the "control points" and the stoppers, the most important diagnostics of the beam lines. The high chamber voltage gradient of 2 kV/2 mm is sustained reliably without arcing. Nevertheless, after months of operation, the high voltage at the detector decreased due to leakage currents caused by silver dendrites growing over the ceramic insulation gaps at the thick film plated foil carriers. This electrochemical migration caused by minimal remnants of hygroscopic solder flux and air humidity was remedied by improved cleaning and using a flow of dry nitrogen (1.5 litre/h) instead of ambient air as the chamber gas. The other thin IC current monitors based on FR4 carriers are not affected and are still operated in ambient air.

At low beam currents, microphonic noise significantly adds to the signal currents of the thin SEM in front of the degrader and averaging would be required for accurate current determination. This is not needed since the SEM is only used as backup to the thin IC monitors for the case of high current densities. Nevertheless, the saturation effects at the IC monitors are lower than expected [2] and hence the SEM can be viewed as solely redundant.

The possibility to adapt the strip configuration of the retractable thick multi-strip ionisation chamber (MSIC) profile monitors to the local beam width proved useful.

## NEW COMPONENTS AND TECHNIQUES

### *Ionisation Chamber Position Monitors*

Three variants of 4-segment IC position monitors (ICPM) will be operated at the PROSCAN beam lines: A conventional IC made from 12 µm thick aluminised Kapton foils with one of the measurement electrodes segmented to 4 quadrants, at the exit of the material irradiation beam line. Non-intercepting position monitors of only 9 mm diameter with intercepting circumferential 4-segment halo monitors, at the control points in front of the gantries [2]. A non-intercepting position and halo monitor at the control point in front of OPTIS 2 (Fig. 2). All are operated with a high voltage of 2 kV in ambient air.

Figure 2: 4-segment ICPM. The electrode configuration from outside to the centre is: ground/high voltage/halo-monitor/position-monitor (= centre electrode). The position monitor covers the full radius of 21 mm, while the halo monitor is fed only from the outer 8 mm. The separatrix splitting the active length of 58 mm between both results from the electric field configuration.

Since the ICPM output depends on the beam size, the absolute position can be estimated only roughly, while the beam centering still can be controlled accurately (Fig. 3).

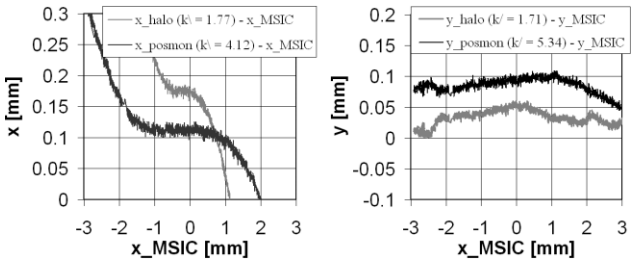


Figure 3: Horizontal and vertical beam position determined from a halo and position monitor of the gantry control point type, referenced to the position from a close-by MSIC. The beam is scanned horizontally. Integration time 20 ms/point. k-values are fitted for horizontal central slopes. (From [2], where erroneously all numbers were shown too large by a factor of 10.) The differences stem from misalignments or errors of the current readings: ±5% current error at the halo monitor or ±3% at the ICPM yields ~±0.1 mm position error in the worst case.

## *Multi-Leaf Faraday Cups*

The beam energy can be determined by a MLFC [3]. After gaining experience with in-air prototypes [4, 5], two variants of in-vacuum MLFCs [6] were built. The latter consist of 64 copper sheets separated by 75 μm Kapton foils and are mounted on compressed-air actuators. The 64 currents are fed to the outside and processed as in the case of the MSIC. Since there is no active cooling, the beam power has to be limited to ~200 kJ/day. Using an electrode at the bottom of the detector head, a voltage pulse can be coupled capacitively to the copper sheets, allowing for a check of the whole system without beam.

The two variants use different sets of sheet thicknesses. Both cover the full energy range of the degrader (Gantry-MLFC: 68 - 252 MeV, Optis-MLFC: 65 - 255 MeV) but the Optis-MLFC uses the thinnest copper sheets of 0.1 and 0.2 mm to improve the resolution in the range of 65 - 85 MeV.

The layout evolved from the following concurrent aspects: The peak should distribute to only a few sheets, giving high enough signals (>>10 pA) even at low beam currents (~500 pA). The ratio of the fwhm peak width $w_{peak}$ to the width of a single sheet $w_{leaf}$ should be larger than 1 for an accurate evaluation (see next chapter). The number of sheets is limited to 64 for a simple realisation.

The total peak width can be estimated from the contributions $\sigma_{stragg}$[mm] = 0.0105 $R$ of the straggling in copper and $\sigma_{beam}$[mm] = 3.2 $dp/p$ $R$ from the beam momentum spread $dp/p$ as $w_{peak}$[mm] = 2.35 $\sqrt{\sigma_{stragg}^2 + \sigma_{beam}^2}$ (with Range $R$ [mm]) [5]. The chosen layouts are depicted by Fig. 4. In the low energy range of the Optis-MLFC the peak-to-leaf width ratio is large enough for an accurate evaluation already at $dp/p$ = 0. For the Gantry-MLFC a $dp/p$ of 0.2 - 0.5% is needed to reach the crucial ratio of 1.

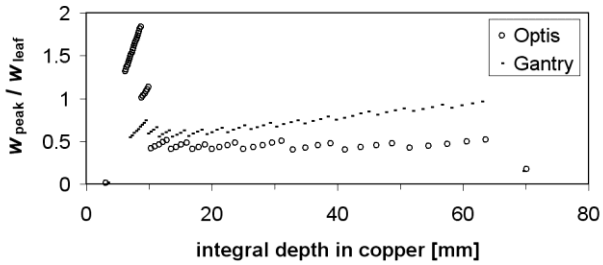


Figure 4: Peak-to-leaf width ratio of the 64 sheets for $dp/p$ = 0. (Data points in copper sheet centres. 75 μm Kapton taken as 16.5 μm copper).

With an assumed overall position accuracy of 0.08 bins (see next chapter) and the given copper sheet thicknesses, the absolute position accuracy of the MLFCs can be estimated. The accuracy expressed in mm $H_2O$ equals roughly the copper sheet thickness in mm at the peak location divided by 2 (Fig. 5). The results for the Optis-MLFC are: 0.05 mm $H_2O$ in the range of 35.5 - 50.7 mm $H_2O$ (65 - 79 MeV) and 0.1 mm $H_2O$ in the range of 50.7 - 58.4 mm $H_2O$ (79 - 86 MeV).

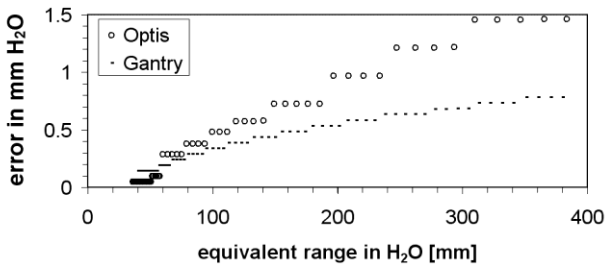


Figure 5: Estimated accuracy of evaluated peak position.

## *Evaluation of Histograms*

Histograms resulting from the measurement of a beam profile with a MSIC or of an energy spectrum with a MLFC are routinely evaluated for beam centre and width. A step-shaped distribution is generated following the shape of the histogram except for the broader outer strips, where a special correction is required. For narrow beams, the beam width calculated from the second moment of the distribution is corrected by an empirical formula [1].

Nevertheless, from the MLFC energy spectra, the underground must be eliminated by ignoring the distribution if it is below a certain cut-off level. Here, the step-shape causes increased errors of position and width and hence a smoother distribution is needed. Nicely smooth area-true representations of histograms are delivered by shape-preserving histopolation algorithms as treated in [7]. On the other hand, the determination of the emittance by the varied-quadrupole method needs a more accurate evaluation of the width of very narrow beams. When this profile width decreases to or below the bin width of the histogram, a priori information on the profile shape is required. Since it is likely that the beam profile resembles a Gaussian, we propose here a "Gaussian histopolation" algorithm. It is based on the fact that for any three positive currents of three contiguous bins (not necessarily of the same width) of a histogram, an area true approxima-

tion by the function

$j(x) = j_0\, e^{-(x-x_0)^2/(2\tilde{s})}$ with $-\infty < \tilde{s}, x_0 < \infty$ and $j_0 \geq 0$

exists. This function is used as a representation for the central bin of the three. An iterative routine is used for each bin to find the parameters $j_0, \tilde{s}, x_0$. Since its present implementation is slow, only off-line evaluations could be done so far. The both outermost bins of the histogram are approximated by a straight line as shown in [1], since this is more reliable in giving a plausible shape than extending the functions of the second outermost bins. Since the algorithm needs non-zero positive bin currents, a minimum bin current is introduced, corresponding to the lower range limit of the logarithmic amplifiers of ~10 pA. In return, the corresponding line current density is subtracted from the resulting distribution.

The algorithm excels in the case of very narrow distributions of nearly Gaussian shape, but is also advantageous in the general case. The fact that the resulting curve is not strictly continuous is of minor importance as long as the beam parameters are derived from moments.

Fig. 6 depicts the evaluation of a simulated distribution (which resembles a MLFC energy spectrum) by the step-shaped distribution ("histogram") and by the Gaussian histopolation, both using a cut-off level of 25% of its peak value. Fig. 7 illustrates the advantage of the smoother distribution. Fig. 8 indicates a position accuracy of the order of ~0.05 bins and a width accuracy of ~20% if the fwhm width of the main peak equals or exceeds the bin width. Error-free current readings are assumed, with a signal sum of 2.5 nA (the beam current of Optis). At very low beam currents (~200 pA), when the 10 pA range limit is not negligible, the errors are larger by a factor of 2 - 3.

For longer integration times (~1s), the accuracy of the current readings of the logarithmic amplifiers depends only on the calibration and the long term stability. With the aspired current accuracy of ±2% [8] the position accuracy decreases to the order of 0.07 bins while the width accuracy is only moderately affected (Fig. 8).

For the MLFC, the individual copper sheet thicknesses have been determined by weighing. The errors introduced thereby are below those from the current measurements.

Similar results were obtained starting from other plausible simulated distributions. An overall accuracy of 0.06 - 0.1 bins can be expected, depending on the current errors.

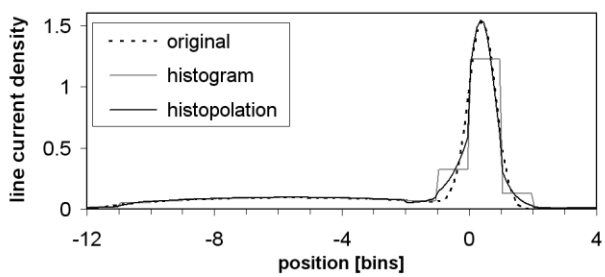


Figure 6: Gaussian histopolation to the histogram of an original distribution (dotted). The fwhm width of the main peak $w_{peak} = 2.35\ \sigma_{original}$ equals the bin width $w_{bin}$.

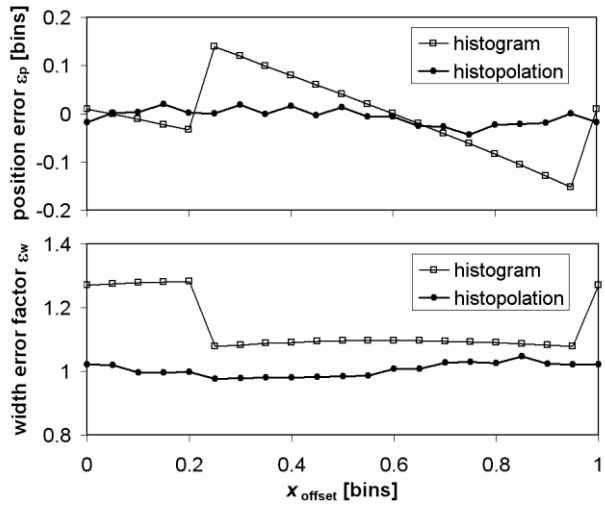


Figure 7a, b: Position error $\varepsilon_p = x_{evaluated} - x_{original}$ and width error $\varepsilon_w = \sigma_{evaluated} / \sigma_{original}$ in dependence on the relative position $x_{offset}$ of the original function of Fig. 6 to the histogram grid.

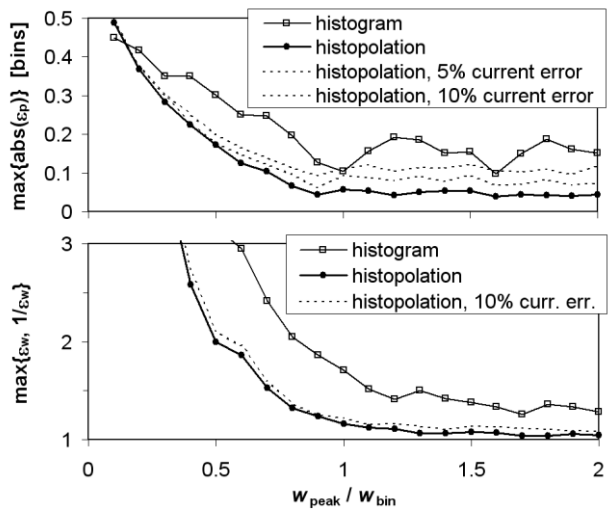


Figure 8 a, b: Maximum position and width errors as from Fig. 7 for a varied width of the main peak of the original distribution. The indicated errors of the histogram bin currents are placed such as to maximise their effect.

## ACKNOWLEDGEMENT

I like to thank M. Rohrer for the thorough mechanical design and R. Erne, G. Gamma and B. Rippstein for mounting and wiring of the MLFCs and ICPMs.

## REFERENCES

[1] R. Dölling, AIP Conf. Proc. 732 (2004) 244.
[2] R. Dölling, AIP Conf. Proc. 868 (2006) 271.
[3] B. Gottschalk et al., Med. Phys. 26 (1999) 2597.
[4] H. Berkhoff et al., PSI Sci. Rep. 2003, vol VI, p. 103.
[5] P. Wittendorp, PROSCAN Docum. P24/WP85-401.
[6] R. Dölling, PROSCAN Document P24/DR84-619.1.
[7] P. Costantini, F. Pelosi, Adv. Comput. Math. 26 (2007) 205.
[8] P. Duperrex et al., AIP Conf. Proc. 732 (2004) 268.